Cytometry PART A
Journal of Quantitative Cell Science

Untangling Cell Tracks: Quantifying Cell Migration by Time Lapse Image Data Analysis

Carl-Magnus Svensson,[1] Anna Medyukhina,[1] Ivan Belyaev,[1,2] Naim Al-Zaben,[1,2] Marc Thilo Figge[1,2]*

[1]Applied Systems Biology, Leibniz Institute for Natural Product Research and Infection Biology, Hans Knöll Institute (HKI), Jena, Germany

[2]Friedrich Schiller University, Jena, Germany

Grant sponsor: Deutsche Forschungsgemeinschaft (DFG) through the excellence graduate school Jena School for Microbial Communication (JSMC) and the CRC/TR 124 FungiNet (Project B4)

Grant sponsor: Leibniz Association through the Leibniz ScienceCampus InfectoOptics SAS-2015-HKI-LWC (Project BLOODi)

*Correspondence to: Marc Thilo Figge, Applied Systems Biology, Leibniz Institute for Natural Product Research and Infection Biology, Hans Knöll Institute (HKI), Beutenbergstrasse 11a, 07745 Jena, Germany Email: thilo.figge@leibniz-hki.de

Published online 4 October 2017 in Wiley Online Library (wileyonlinelibrary.com)

DOI: 10.1002/cyto.a.23249

Abstract

Automated microscopy has given researchers access to great amounts of live cell imaging data from in vitro and in vivo experiments. Much focus has been put on extracting cell tracks from such data using a plethora of segmentation and tracking algorithms, but further analysis is normally required to draw biologically relevant conclusions. Such relevant conclusions may be whether the migration is directed or not, whether the population has homogeneous or heterogeneous migration patterns. This review focuses on the analysis of cell migration data that are extracted from time lapse images. We discuss a range of measures and models used to analyze cell tracks independent of the biological system or the way the tracks were obtained. For single-cell migration, we focus on measures and models giving examples of biological systems where they have been applied, for example, migration of bacteria, fibroblasts, and immune cells. For collective migration, we describe the model systems wound healing, neural crest migration, and *Drosophila* gastrulation and discuss methods for cell migration within these systems. We also discuss the role of the extracellular matrix and subsequent differences between track analysis in vitro and in vivo. Besides methods and measures, we are putting special focus on the need for openly available data and code, as well as a lack of common vocabulary in cell track analysis. © 2017 International Society for Advancement of Cytometry

Key terms

biomedical image processing; cell migration: track analysis

THE migration of cells is an essential process in biology and a key factor in physiological events such as development (1,2), regeneration (3,4), and immune response (5–7). In disease, the movements of bacteria (8–11), amoeba (12,13), and cancer cells (13–18) have been tracked and analyzed. With a steady development of microscopy techniques, it has become possible to image individual cells over long periods of time both in vivo and in vitro. In vitro experiments are normally done assuming that cells move in two dimensions (2D) (19,20), while in vivo imaging normally captures the actual three dimensions (3D) of the organism (21,22). Modern microscopy techniques, such as light sheet microscopy, can produce data with speed of up to 1 GB/s (23) giving amounts of data that are unfeasible for manual analysis (24). Because of this, the area of automated image analysis in general and tracking in particular is a very active field of research (5,25–28). This review is mainly concerned with the steps that occur after the tracks are acquired, namely the quantitative analysis of the tracks. We provide an overview of what measures and models are being used and some model systems that are routinely investigated. This review focuses on analysis of migration patterns, that is, what is the migration behavior that is observed by just analyzing the tracks, not the motility mechanisms of cells. For an overview of the mechanisms of migration, or migration modes, we refer the readers to a recent review by Blanchoin et al. (29). Also, the modeling of cell motility (30) and models of how cells locally react to chemoattrac-

Glossary

Collective migration: Migration of cells where the individual cells are strongly influenced by their environment and/or other cells.
Chemotaxis: The movement of cells that is influenced by a chemical stimulus. Following chemotactic signals is for example used by bacteria to find food or by neutrophils to migrate to sites of inflammation.
Diffusivity: Squared distance per unit time that a molecule or object will on average move due to Brownian motion. Diffusivity is denoted by the diffusion constant D.
Directional bias: The case of movement not being isotropic but following a preferred direction, denoted by $\boldsymbol{u}$.
Extracellular matrix (ECM): Tissue network surrounding cells in organs that provides structural support, tissue segregation and regulates intracellular communication. The ECM structure and composition strongly depends on the type of the tissue: from the stiff minerals of bone ECM to the liquid plasma that is the ECM of blood.
Hidden Markov model (HMM): A model where the observable data is caused by hidden states. The hidden states are assumed to be Markovian, i.e. the transition to the next state only depends on the current states and has no memory of earlier states.
Intravital microscopy: Collective name for acquisition of microscopy images in vivo. The modality of microscopy varies depending on the transparency of the tissue but the most common types are multi-photon microscopy, confocal microscopy and fluorescence lifetime imaging microscopy (FLIM).
Isotropic and anisotropic environment: Isotropic is an environment that is identical in all directions from a given point. An anisotropic environment lacks this property; a relevant example of an anisotropic environment would be an extracellular matrix with a lot of structure in a preferred direction.
Monte Carlo simulation: A method of random sampling that is applied, among other things, to draw samples from a distribution that need not be well described by analytical functions. Such a distribution can, for example, be a complex turning angle distribution that was recorded from a cell population (79). The turning angels are then randomly sampled from this distribution to create synthetic tracks.
Persistence: The time period during which a cell moves in the same direction. From a mathematical point of view this is described as the correlation length of the velocity during subsequent time steps. Persistence is denoted by τ.
Posterior PDF: Distribution of parameter values determined using Bayes formula, posterior PDF $\propto$ likelihood $\times$ prior. This approach allows for a hypothesis (prior) to be supported or rejected based on the probability of seeing the data (likelihood).
Probability density function (PDF): Function that is connected to a specific continuous probability distribution. When integrated between two limits, PDF gives the probability of the stochastic variable to be in that range. For discrete probability distribution this is known as the probability mass function (PMF).
Segmentation: The image analysis process that identifies objects, for example individual cells, in an image.
Single cell migration: The movement of single cells that can be considered independent of the actions of other cells. Chemotaxis is normally considered to be single cell migration as long as the migrating cells are not strongly influencing each other.
Track (Trajectory): A time-ordered set of coordinate points that is the basis for track analysis.
Tracking: The task of following an individual object or part of the image across numerous time frames.

tant (31) are subjects that are beyond the scope of this review. Although in track analysis, just as in automated image analysis in general, tailor-made algorithms and analysis pipelines are often needed, we try to summarize the state of the art and identify open questions and challenges. In this review, we also try to clear up some nomenclature issues for methods and measures. As the same measure may be called differently in different publications, the lack of a common vocabulary is a real issue in track analysis (32) and, here, we at least point out some common ambiguities.

For track analysis to be meaningful, the tracks have to be correctly obtained and recorded. In their review, Beltman et al. (5) point out issues and suggest corrective measures to problems such as tissue drift, errors at the edge of the field of view, and longer tracking time of slow moving cells. In this review, we focus on the analysis downstream from a successful cell tracking procedure. However, for a complete picture, we first give a brief overview of the main tracking approaches. We then move on to single cell migration and introduce measures and models that are used to analyze cells that migrate with little interaction with each other. Here, the focus is on methods rather than systems, even if we refer to practical examples where different measures and models were used. We also discuss collective cell migration, where we focus on a few biological model systems rather than methods as the measures used are quite intuitive and simplistic, whereas the models and reasons for investigating the migration are highly system specific. Next, we address the role of the extracellular matrix (ECM) whose properties are extremely important when tracking cells in vivo. We close the review by discussing perspectives and challenges in cell track analysis.

Tracking

While tracking is not the main focus of this review, we briefly describe the most common methods and challenges in automated and semi-automated tracking. Much literature is concerned with tracking in the fields of general computer vision (33–35), tracking of cells (20,36), and particles (37–41). Tracking algorithms can roughly be divided into the following three categories: tracking by detection, tracking by model evaluation, and tracking by filtering (20). Tracking by detection is the most common approach where individual objects are detected by segmentation (20,26) in each frame, and the objects are then matched across frames. This method has been used to track many different cell types including immune cells (7,42) and cancer cells (43,44). Segmentation is the task of identifying all individual foreground objects in a single image. After the segmentation step, the tracking is performed by identifying the same cell in subsequent frames, thereby linking the cell positions across time frames. Besides difference in cell segmentation methods, various methods exist to link the objects across frames, which is an optimization problem that

has to be solved (45). One common approach is to minimize the global cost of Euclidian displacements either across the entire image (37) or in local cell clusters (42,46). Other approaches include integer programming (44), multiple hypothesis tracking (47), and dynamic programming (48).

Tracking by model evaluation utilizes active contours to track cells and has been successfully applied to immune cells (49,50), cancer cells (51), fibroblasts (52), and amoeba (53). Active contours deform and translate the zero crossing of an energy functional to minimize its energy based on external and internal energy terms (54). External energy depends on image properties such as pixel intensity and the occurrence of gradients, while internal energy terms are, for example, the enclosed area and circularity of the contour. Active contours rely on initial conditions that are close to the true solution. If the frame rate is high enough the solution from the previous frame is often a good enough choice (20,54); however, it is not unusual that manual adjustments are necessary to obtain satisfactory initial conditions from the first frame (11,55).

Tracking by filtering approaches are probabilistic by nature and particularly popular in the tracking of virus particles, which is a challenging problem due to the low signal to noise ratio (38,41,56). The most common filtering approach is particle filters, which is a numerical approximation of the Kalman filter using a hidden Markov model (HMM) to approximate the future posterior probability density function (PDF) for object positions based on the current posterior PDF (57,58). The PDF is weighted with the latest measurements, that is, the new frame, to determine the most probable positions of the objects.

Independent of the method of tracking and system of interest, we define a track as a time-ordered set of points $\bar{\boldsymbol{x}}=[\boldsymbol{x}_1, \boldsymbol{x}_2, \ldots, \boldsymbol{x}_N]$, where the subscript indicates the time point, i, at which the position $\boldsymbol{x}_i$ was recoded. We assume that we have N time points and each position is either in a 2D or 3D coordinate system. Dependent on the tracking method, additional information like the size and shape of cells may be provided. Normally, we will not assume that such information is available, but if we discuss an analysis method that explicitly requires anything besides the cell positions, this will be mentioned.

Single-Cell Migration

Cell Track Measures

What characteristics should be used when describing a track? From an intuitive point of view, the speed and direction are the two measures that describe any motion. Unfortunately, cells are normally not moving between two points along a straight line with constant speed. There are multiple reasons for this, for example, geometrical constraints (59,60), multiple directional cues (61,62), and simply that the cell is searching the space in the absence of signals (63). Measuring the instantaneous speed of a cell also suffers from the issue of finite sampling frequency and we cannot know the positions of the cell between frames (64). An investigation of the identical system with a different frame rate would then give differences in measured speed values. It has been suggested that the frame rate should be tuned so that cells move less than their diameter between frames (65). In systems with heterogeneous movement patterns between cells or over time, this may not always be realizable.

In Figure 1, we plotted synthetic tracks for three different conditions, which will be used to exemplify how some different track types translate into different measures. When generating the tracks, we have changed the persistence of the tracks, denoted by τ, and the directional bias denoted by $\boldsymbol{u}$. We define the persistence time as multiples of a time step in arbitrary units. The tracks were generated by simulations of the differential equation

$$\frac{d\mathbf{v}(t)}{dt} = -\frac{1}{\tau}\mathbf{v}(t) + \frac{\sqrt{2D}}{\tau}(\mathbf{n}(t) + \boldsymbol{u}), \qquad (1)$$

where the vector $\mathbf{v}(t)$ is the velocity vector and $\mathbf{n}(t)$ is added white noise. Apart from the bias term, Equation (1) corresponds with the Langevin equation in dimensionless units (mass, length, and timescales are set to 1) (66,67). This is commonly used in persistent random walk (PRW) models, which we discuss in more detail later. The diffusion constant D describes the overall diffusivity of the system and for our generated tracks this is set to $D=\tau^2$ so that the persistence does not change the overall contribution of noise to the cell track. The tracks generated with $\tau=3$ will be referred to as the

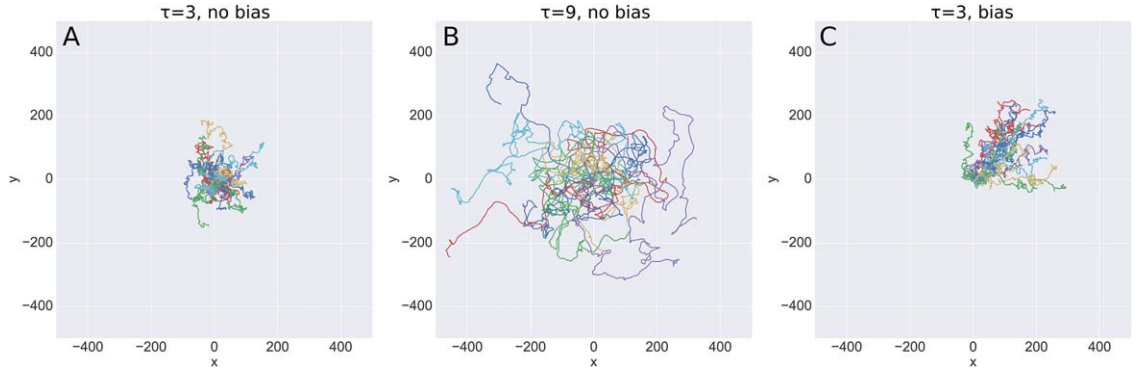

Figure 1. Synthetic tracks generated with different parameters to demonstrate the possibilities and limitations of track analysis. In (**A**), the tracks have a low persistence and no directional bias and, in (**B**), the persistence is increased. In (**C**), the persistence is the same as in (A), but a directional bias toward the upper right corner was introduced.

Table 1. Some of the most commonly calculated track measures

MEASURE	DEFINITION
Distance between track points	$d(\boldsymbol{x}_i, \boldsymbol{x}_j) = \sqrt{\sum_{d=1}^{D} (x_{i,d} - x_{j,d})^2}$, where D is 2 or 3
Total distance	$d_{\text{tot}} = \sum_{i=1}^{N-1} d(\boldsymbol{x}_i, \boldsymbol{x}_{i+1})$
Net distance	$d_{\text{net}} = d(\boldsymbol{x}_1, \boldsymbol{x}_N)$
Max distance	$d_{\max} = \max_i(d(\boldsymbol{x}_1, \boldsymbol{x}_i))$
Mean-squared displacement (MSD)	$\text{MSD} = \frac{1}{N-1} \sum_{i=1}^{N-1} d(\boldsymbol{x}_i, \boldsymbol{x}_{i+1})^2$
Meandering index	$\text{MI} = d_{\text{net}} / d_{\text{tot}}$
Outreach ratio	$\text{OR} = d_{\max} / d_{\text{tot}}$
Instantaneous velocity	$\boldsymbol{v}_i = \frac{\boldsymbol{x}_i - \boldsymbol{x}_{i+1}}{\Delta t}$, where Δt is the time between frames
Instantaneous speed	$v_i = \lvert \boldsymbol{v}_i \rvert$
Velocity autocorrelation	$v_{i,j}^{\text{ac}} = \boldsymbol{v}_i \boldsymbol{v}_j, \quad i > j$
Global turning angle (2D)	$\alpha_i = \tan^{-1}\left(\frac{x_{i+1,2} - x_{i,2}}{x_{i+1,1} - x_{i,1}}\right)$
Relative turning angle	$\varphi_i = \cos^{-1}\left(\frac{\boldsymbol{v}_i \cdot \boldsymbol{v}_{i+1}}{\lvert \boldsymbol{v}_i \rvert \cdot \lvert \boldsymbol{v}_{i+1} \rvert}\right)$
Direction autocorrelation	$\text{DA} = \cos(\alpha_{i+1} - \alpha_i)$

nonpersistent cells (Fig. 1A) and the ones with $\tau = 9$ as the persistent cells (Fig. 1B). The case of $\tau = 3$ and directional bias (Fig. 1C) will be called the directionally biased cells. The bias was implemented by setting $\boldsymbol{u} = (0.1, 0.1)$ in the case of directionally biased cells and $\boldsymbol{u} = (0.0, 0.0)$ otherwise. All other parameters are identical, and all tracks are starting at position $(x,y) = (0,0)$ with random initial velocity. For each condition, 200 tracks with $N = 500$ steps were generated and, in Figure 1, we have plotted 20 randomly chosen tracks from each condition. The persistence describes the dependence of velocity on the previous velocity and gives straighter tracks when increased, as can be seen when comparing Figure 1A,B. In Figure 1C, we have plotted tracks that have a directional bias toward the upper right corner of the plot, while the persistence is the same as in Figure 1A. This is done to simulate a chemotaxis experiment. Track simulations, measure calculations and visualizations are made using a customized Python script, which is available under https://asbdata.hki-jena.de/publidata/SvenssonEtAl2017_CytoA/SvenssonEtAl_CytoA_2017.zip. In the pack, videos of selected tracks for the three conditions are also included.

In Table 1, we have listed some of the measures that are most commonly calculated when evaluating cell tracks (5,20,65,68,69). To illustrate some of the most basic measures, we have plotted a track in Figure 2 with net displacement (d_{net}), max displacement ($d_{\max}$), global turning angle (α_3), and relative turning angle (φ_2) specially marked. The most used measure is probably the mean-squared displacement (MSD). MSD is actually a special case of larger family of measures referred to as moment scaling spectrum (70) defined as

$$\text{MSS} = \frac{1}{N-1} \sum_{i=1}^{N-1} d(\boldsymbol{x}_i, \boldsymbol{x}_{i+1})^p, \qquad (2)$$

where p is an integer larger than zero. If $p = 2$, we get the MSD, but general formulations where p is allowed to vary have been applied to analyze tracks of viruses and virus-like particles (37,71). As the MSD describes the diffusivity of a cell or a system, it is common to fit cell migration models, such as the Langevin equation that we have already introduced (Equation (1)), to the MSD to quantify differences between cells or populations (72). In a system with purely random motion, so-called Brownian motion (72), it is known that the value of MSD is proportional to time. If the MSD is evolving faster, then the system is called super diffusive and the cells are moving in a more directed fashion than is expected from a purely random walk. If the MSD instead evolves slower than MSD $\sim t$, the movement is called sub-diffusive and the cells are then spatially more confined than expected for Brownian motion. MSD, just as most other measures, does not uniquely describe the migration mode of cells. For example, it has been shown for T cells migrating in lymph nodes that different movement types may give similar MSD characteristics (5). In

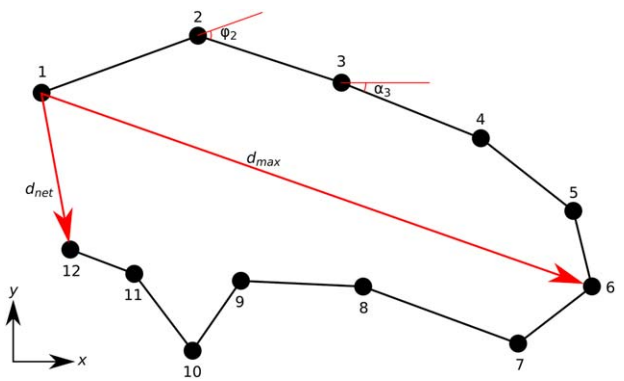

Figure 2. One example track with $N = 12$ steps in 2D with some of the measures from Table 1. We have marked net displacement (d_{net}), max displacement ($d_{\max}$), global turning angle (α_3), and relative turning angle (φ_2).

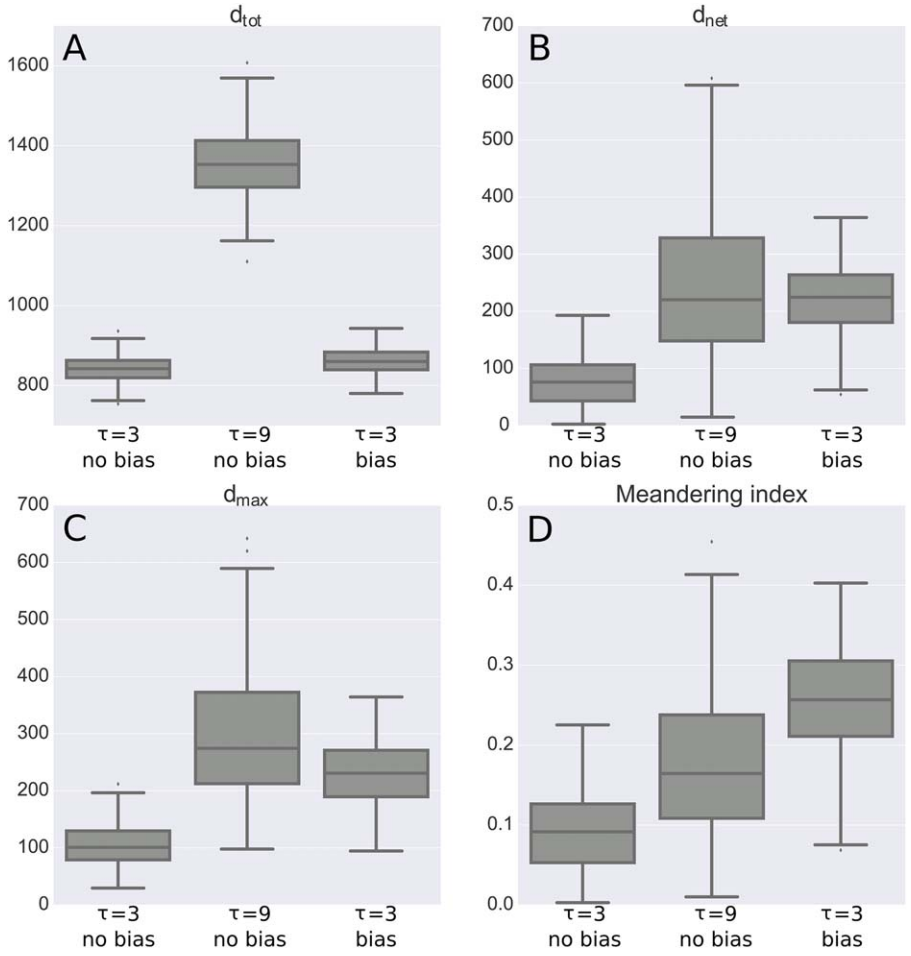

Figure 3. Some of the measures from Table 1 plotted for the three migration cases shown in Figure 1.

section "Cell Migration Models," we explore such models and how they make use of the MSD in more detail.

Quite often one or more measures are used to directly quantify differences between conditions that are suspected to affect migration patterns. A nice example is the study by Huang et al. (13) where speed, meandering index (see Table 1), and MSD were used to examine breast cancer cell chemotaxis under different flow conditions. Instead of meandering index, Huang et al. refers to the ratio d_{net}/d_{tot} as persistence, which in general is a term that is used to describe continuous movement in a certain direction during an uninterrupted period of time. Besides the terms meandering index and persistence, the names linearity, straightness index, and confinement ratio are also used for the same measure (20,73–76). Naturally, this is confusing for the reader who may not realize that the same measure is used in two separate studies or think that two nonidentical measures are actually the same. An example of the latter would be the confusion between meandering index and persistence that we exemplified (13). Meandering index was directly used to investigate the effect of the CCR7 ligand on the motility of T lymphocytes (77) and B lymphocytes (78), to derive a migration model for germinal center B cells from intravital microscopy data (79,80), and to study the migration of epithelial cells during morphogenesis under different conditions (74). The meandering index was in these studies supplemented by additional measures such as velocity, relative turning angles, total displacement, and net displacement (see Table 1 and Figure 2 for definitions).

In many cases, a single measure is simply not sufficient to accurately and uniquely describe the system dynamics. Figure 3 demonstrates the need to consider multiple measures by showing total distance, net distance, max distance, and meandering index for the three migration cases from Figure 1. The difference between the nonpersistent unbiased and persistent tracks is clear in all four measures; the persistent ones have a considerably higher net distance and higher meandering index. However, when distinguishing between the biased migration and the other cases the picture becomes more complicated. The biased cells have a higher meandering index than the persistent cells and a similar net displacement. However, when considering the variability of the distribution of measures across tracks as well as the total displacement, the biased cells are quite similar to the non-persistent cells. By simple investigation of the migration plots in Figure 1, it is

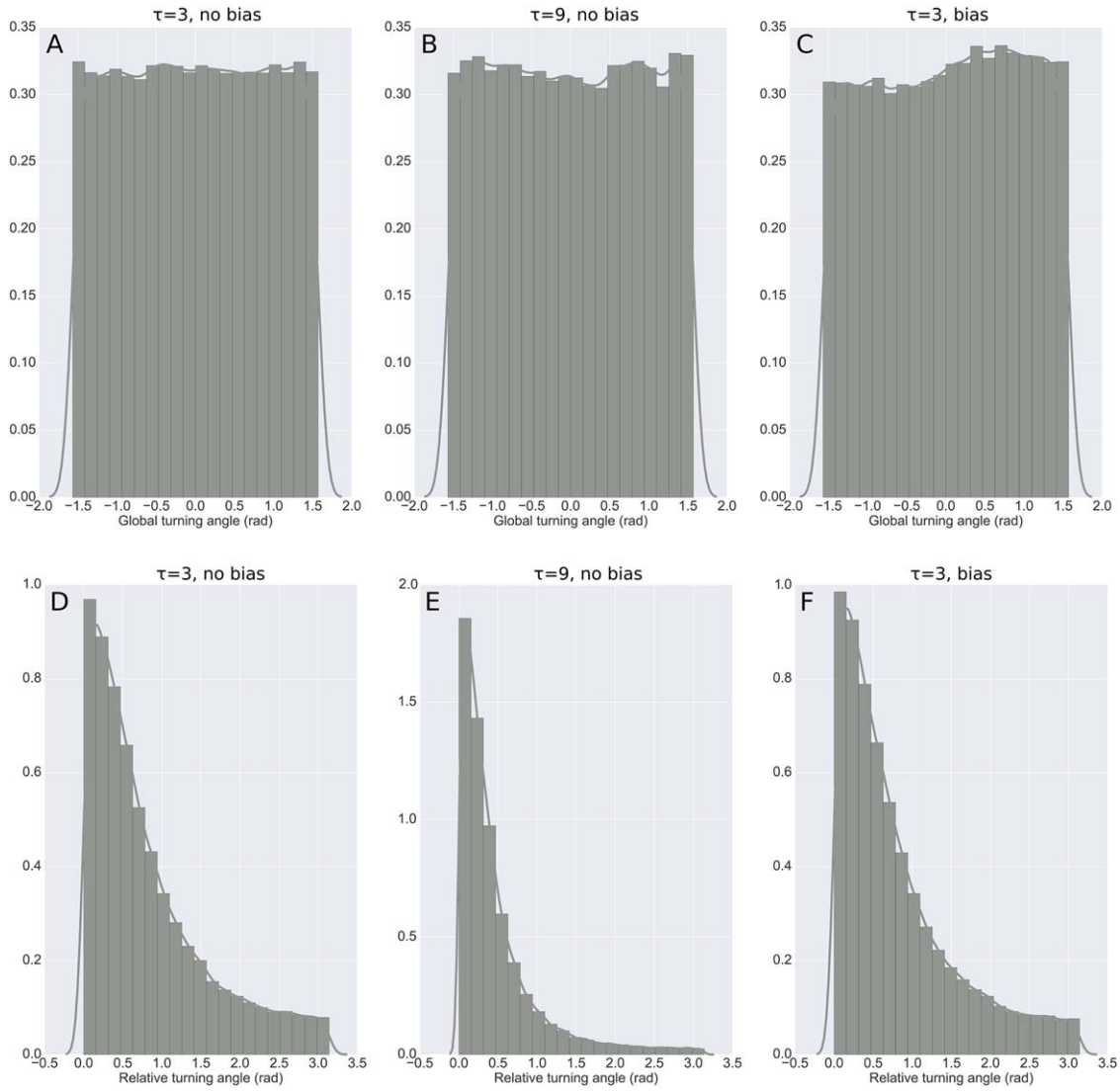

Figure 4. Histograms of global turning angles (**A**–**C**) and relative turning angles (**D**–**F**) for the tracks shown in Figure 1.

easy to see that the three cases have very different migration properties, while from the measures in Figure 3, these differences are much more obscure. The total displacement measure indicates that the two cell populations with $\tau=3$ are similar, but there is a lack of information that a directional bias is the reason for differences in the other measures. By just considering the net distance, the directed cells and the persistent cells have travelled a similar distance, while the nonbiased, nonpersistent cells are more confined in their migration. If we then add the fact that the persistent cells have a considerably higher total distance travelled than the other two cases we can conclude that the persistent cells are more diffusive and that leads to the high net distance. The reason for the high net distance of the biased cells is rather because they are walking straighter which is then supported by the high meandering index of these cells. This is just an example on how knowledge about cell migration can be extended by considering more and more measures.

Another characteristic of cell migration, the turning of cells, is often calculated in two different ways namely relative and global turning angle, denoted α and φ, respectively. In Figure 2, we have illustrated how the two types of angles are calculated and the formulas for both measures are listed in Table 1. Confusingly, both are from time to time simply referred to as "turning angle," which is another example of the lack of controlled vocabulary in track analysis. The global turning angle describes the angles with respect to the fixed coordinate system giving information about the global influences (65). Figure 4A–C shows histograms of the global turning angle for the three cases of synthetic tracks plotted in Figure 1. There is no difference in the global tuning angle between the nonpersistent and persistent tracks (Fig. 4A,B, respectively), but the case with a directional bias (Fig. 4C) clearly shows a preference to turn in toward the upper right corner of Figure 1C ($\alpha = \pi/4$). The relative turning angle describes how much a track deviates from its previous

direction and is used as a measure of persistence (76). Here, we see a clear difference between the nonpersistent cells and the persistent ones (Fig. 4D,E). In the case of biased migration (Fig. 4F), the distribution reverts back to the one given by the nonpersistent cells without any bias. This nicely demonstrates the importance of adapting the choice of measures based on specific questions that are to be answered. Thus, the global turning angle distribution gives information about biases, which can be important in chemotaxis experiments, while the relative turning angle distribution is more informative to characterize cell persistence.

A measure that can be useful in chemotaxis experiments is the forward migration index (FMI) that describes the direction toward such a chemotaxis source by leukocytes (61). The FMI takes the ratio between the progress in the "correct" direction by a cell and the total distance. Such a measure requires that it is known what this correct direction is. Normally, anisotropic movements are elucidated with the help of rose plots or angular plots (20,81), as can be seen in Figure 1. Such plots are often complemented with other measures to give a complete idea about the migration patterns (74,82).

Often the measures listed in Table 1 are supplemented by less common measures or measures that are specific for the system in question. For instance, Mokhtari et al. (76) use the already defined meandering index and outreach ratio together with the asphericity, displacement ratio, and volume prolateness (only 3D) to describe the migration patterns of synthetic tracks as well as neutrophil tracks. Besides the combination of track measures the authors introduce staggered versions of measures creating heat maps where each track point is treated as a start point and the measure evolves both forward and backward in time. The staggered version of the measure is thereby able to visualize both global and local behaviors of each track. However, one possible drawback of staggered measures is that for each track, an order of N^2 numbers has to be calculated, which may be computationally expensive if each track has several hundred track points. An example of a system-specific measure is the investigation of sperm quality under heavy metal exposure (73). Besides a number of already mentioned measures the amplitude and beat frequency of the sperm head is recorded. These are naturally measures that are only possible to obtain for organisms that perform such actions. Other measures require additional information than is normally provided by standard tracking methods. An example of this is the cell migration potential index (CMPI) (83). The CMPI is based on the movement of the cell nucleus within the cell, that is, whether the nucleus position is fixed or fluctuating with regard to the cell center. This naturally requires that the cell nucleus can be distinguished within the cell and that the outline of the cell can be accurately segmented. This is not a standard procedure in tracking and for certain cells, such as neutrophils, the "nucleus" has a quite irregular shape, which would make this type of analysis extremely challenging.

In conclusion of this section, we note that there are almost as many measures and names as there are studies. Some measures, such as meandering index and MSD, are more common than others. Almost all measures focus on distances between well-chosen track points, velocities, and turning angles. Two of the most commonly calculated measures, MSD and turning angle distribution, are not only used for direct analysis but also for fitting statistical models that we focus on in the next section. As can be seen for our example tracks from Figure 1, great care has to be taken when deciding what measures should be calculated and often a combination of measures is necessary. As can be seen in Figure 1, it is also of great importance to visualize the tracks to be able to detect qualitative characteristics and thereby being able to interpret the measures in a meaningful way.

Cell Migration Models

An alternative to direct use of measures as descriptors of cell motility is to describe the movement with the help of a migration model. Different motility patterns are then distinguished by different parameter values or by the identification of a model that best describes the current cell system. Advantages of the model approach are that the differences normally are in the low dimensional space of the parameters of the model and that the interpretation of differences is straightforward. Cell tracks are intrinsically noisy and it is therefore natural to use stochastic models to quantify their movement. The most basic stochastic model for purely random motion is the Brownian motion, which was mathematically first described by Einstein in 1905 (84). Soon it was discovered that biological systems did not follow a Brownian pattern as most cells have a directional persistence (85,86). This gave rise to the PRW model that still is the basis of most studies that analyze cell motility using stochastic models. This model is sometimes also referred to as a correlated random walk (72). The base model for PRW is the Ornstein-Uhlenbeck (OU) process that is satisfied by the Langevin equation, given by Equation (1) with $\boldsymbol{u}=(0.0, 0.0)$. The parameters that are then fitted to data are the persistence time, τ, and the diffusion coefficient of the Brownian motion, D (64,66,67). A very attractive aspect of the OU process is that the parameters can be determined by considering the observable measures MSD and velocity autocorrelation (see Table 1 for definitions). The OU process has been used to describe the motion of microvessel endothelial cells (87), lung epithelial cells (15), the twitching motion of the bacterium *Neisseria gonorrhoeae* (88), and the locomotion of fibroblasts (89). However, the OU process assumes that the noise is normal distributed with a zero mean, which is an assumption that is not always fulfilled both in 2D (63,90–92) and in 3D (93). To model a PRW without this limitation, other tractable models have been developed that do not rely on a white noise model. An example is the model derived for monolayer forming HaCaT cells by Selmeczi et al. (90), where the model was derived from data and basic principles. Example of such a basic principle is that the velocity autocorrelation function is part of a family of functions with exponential decay when the time period between time steps i and j increases. This model system has up to seven parameters, thereby losing the property of a compact representation of motility by the OU process. The PRW model has also been

used to describe B cells in the germinal center by Figge et al. (79), where the speeds and turning angles were obtained from data and the model was realized by Monte Carlo simulations to avoid assumptions about the noise model. Also, Huang et al. (94) used Monte Carlo simulations to show that the intrinsic motility characteristics of fibroblasts change based on their current role in tissue patterning.

A popular approach for modeling optimal search patterns of both animals and microbes is the scale free Lévy walk (9,95,96). Lévy walks are characterized by a stop-start pattern where the cells are more or less stationary for some time followed by a directed walk of length L, where L follows a power law distribution, $P(L) \sim L^{-\mu}$ with $1 < \mu < 3$. In a Lévy walk, directed migration is represented not by a number of subsequent steps with the same direction, but by one jump with length L. Lévy walks in cell migration were first observed for *Escherichia coli* by Berg and Brown (8), and the movement pattern was described by the term "run-and-tumble". In some other works, the same type of movement pattern has been described by the term "stick-and-slip" (67,86). Lévy walks have also been used to describe the movement of epidermal cells (90) and CD8+ T cells (97). However, the application of the Lévy walks is not uncontroversial; it has been suggested that the Lévy walk is not at all optimal (98,99) and that the entire idea of the model is not biologically plausible (98,100), partly because a pure Lévy walk requires infinite step lengths to be possible. Infinite step lengths are not realistic from a biological perspective and even if present they cannot be observed as the time and field of view are both limited (101). Instead, models such as the composite persistent random walk (CPRW) have been suggested as alternatives (102). The CPRW is driven by Langevin type equations, see Equation (1), where the noise model is implemented by quite exotic distributions such as von Miese, wrapped Cauchy, and Weibull distributions (102,103). In response to this criticism, it has been suggested that individuals that perform a PRW in isolation may take on Lévy walk behavior when moving in swarms (104,105). For *E. coli*, the superposition of different exponential noise distributions affecting enzyme receptors gives rise to Lévy walks also for individual cells (106). The validity of the Lévy walk description of motion is an active discussion among researchers in biology and ecology (95,99,100,105,107), and part of the issue is that from an observable, normally a collection of tracks, both Lévy walks and CPRWs fit equally good at first glance. Work has been done to quantify which is the better description (102), but this is normally focused on specific data sets that may not allow for general conclusions.

The stochastic models described so far assume an isotropic environment, that is, the cells are equally likely to migrate in each direction. Models have also been used to investigate motility in chemotaxis experiments, for example, the movement of *Dictyostelium* amoeba in shallow gradients (108) and leucocyte migration toward sites of injury (109,110). The simplest model for motion that is affected by an external signal is the biased random walk (BRW) in which the drift-diffusion equation is used as a model (72,79,80,111). The general drift vector can then be determined by fitting the data to the model and a general bias in movement can be detected. This type of modeling has been used to find biased motion of leucocytes (109) and T cells (112,113). The BRW lacks any type of persistence in its formulation; nevertheless, it may be used to describe biased motion. The expectation values of the total displacement and MSD at time t under the BRW assumption are

$$E[d_{\text{tot}}](t) = \boldsymbol{u}t \tag{3}$$

and

$$E[\text{MSD}](t) = |\boldsymbol{u}|^2 t^2 + 4Dt, \tag{4}$$

where $\boldsymbol{u}$ is the drift vector that describes the bias and D the diffusion coefficient. If we fit D and $\boldsymbol{u}$ to the synthetic track data plotted in Figure 1, we get the values that are listed in Table 2. The values for diffusion, D, and the length of the bias vector are naturally over-estimated as the BRW has no persistence. In Figure 5, we have plotted the fit of Equation (4) and the MSD from the synthetic tracks and we see that we have good fits, even though there is no persistence. It is however worth noting that the diffusion parameter is equal between the cases that have $\tau = 3$ whether there is a bias or not. Similarly, both the nonbiased case with $\tau = 3$ and the nonbiased case with $\tau = 9$ display a drift vector much closer to [0,0] compared to the drift vector of the biased tracks. This shows the strength of the BRW as we can apply it to data that are created with a different mechanism and it is still able to distinguish between the biased and unbiased migration processes. A very nice example that combines direct analysis of migration measures (e.g., MSD), BRW, and the simulation of different types of tracks is the article by Textor et al. that investigates whether T cells in the lymph node are random or directed walkers (112).

Table 2. The fitted BRW model parameters D and $\boldsymbol{u}$ for the three migration types plotted in Figure 1

MIGRATION TYPE	DIFFUSION, D	BIAS VECTOR, $\boldsymbol{u}$
$\tau = 3$, no bias	4.4	[–0.02, 0.01]
$\tau = 9$, no bias	42.3	[0.02, 0.02]
$\tau = 3$, bias	4.6	[0.30, 0.29]

To analytically solve a biased persistent random walk (BPRW) is possible in one spatial dimension by solving the one dimensional telegraph equation (70). In 2D, which is normally the lowest dimension on which cell tracks are analyzed, the telegraph equation is solvable, but it is not the asymptotic solution of a BPRW. This means that fitting the telegraph equation in 2D to a system where cells perform a BPRW, the parameters do not describe the system behavior in terms of bias and persistence, that is, if the bias was removed the remaining persistence value would not describe the movement of cells. Lately, theoretical works have been published that investigate the asymptotic behavior of BPRWs (114–116), but to date, this has not been used to describe cell motility. Instead, BPRWs have been modeled by ad hoc models very much tailored to the particular system with the geometry of the experiment as a significant part of it. An example thereof

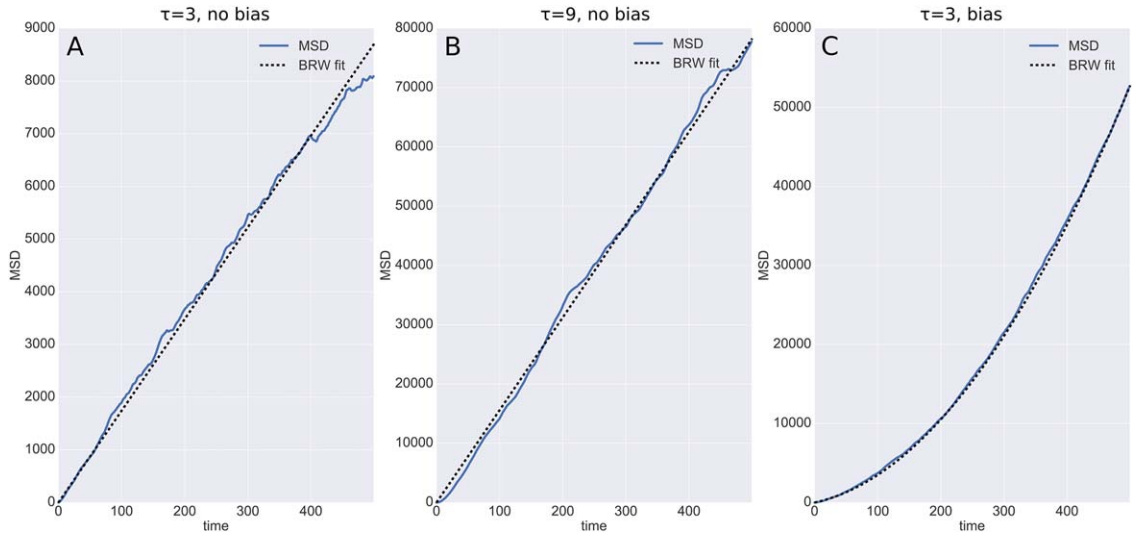

Figure 5. The MSD and fitted BRW, Equation 4, for the three migration cases from Figure 1. In (**A**), the MSD for cells with τ=3 and no bias, in (**B**), the persistent cells with τ=9, and finally in (**C**), the biased cells with τ=3.

is the study of Hill and Häder that investigate the trajectories of algae under phototaxis (swimming toward a light source) and gyrotaxis (movement caused by gravitational forces) (117). The targets causing the directionality of the algae, that is, the light and gravity, are in the model assumed to be uniform and placed at infinity, giving von Miese type steady state distributions for the movement of algae. In many chemotaxis experiments, the position of the chemotaxis target is known and the chemotactic effect is not uniform across the entire field of view. Because of these limitations and the usefulness of the BRW approach even for cases with persistence, as described in Figure 5, the BRW is currently a much more used model, even though it clearly does not capture the persistence property of cell migration. For a more detailed description of random walk models in general and possible solutions to the BPRW problem in particular, we would like to refer the reader to the excellent review by Codling et al. (72).

Heterogeneous Populations

Biological data, including cell tracks, naturally show a wide range of variability. When fitting a model or calculating a measure to describe an entire population of cells, one type of behavior is attributed to all of them. Recently, the heterogeneity of cells within populations and even the switches in migration behavior of single cells, temporal heterogeneity, have become a subjects of interest (76,93,109,113,118–121). Using direct measures on single tracks, studies have attempted to describe this heterogeneity in different populations. We have already described the study by Mokhtari et al. (76), which used a collection of staggered measures to discriminate between tracks of a confined nature and straight walkers. In model-based analysis, it has been suggested that PRW is a complete model for cell motility in 2D as long as cell population heterogeneity is taken into account (93,119). Temporal heterogeneity has been studied in the light of cell interactions with the environment (120) and stochastic levels of signaling proteins (109,121). Due to the limited field of view, and thereby limited time of tracking, switches in migration behavior can be hard to detect, but lately technical improvements for in vivo imaging have allowed such behaviors to be detected for T cells (113) and leukocytes (109,122).

An attractive framework for capturing heterogeneity both in time and space is presented by Metzner et al. (118) where they use a first order autoregressive process (AR-1), which is defined by

$$\boldsymbol{v}_i = q_i \boldsymbol{v}_{i-1} + a_i \boldsymbol{n}_i. \quad (5)$$

Here, the velocity vector, $\boldsymbol{v}$, is determined for each time point i. The magnitude and sign of one parameter, q_i, in this model can make the cells follow a PRW, a Brownian pattern or anti-persistent motion. The analysis of this model is done by inferring the posterior PDF $p(q, a)$ using Bayesian update rules. The PDFs for three different environments, consisting of collagen, plastic or fibronectin, were shown to be clearly different (118).

Collective Movement

So far, we have assumed that every cell is migrating individually. During chemotaxis, each individual cell follows an existing gradient independently whether the cell is completely isolated or surrounded by other cells that are affected by the same gradient. However, in many situations, this assumption does not hold and cells move collectively based on environmental effects and cell-to-cell interactions. Collective migration is an extremely important feature in developmental biology, regeneration, and morphogenesis (2,60,123). In collective motion, the tracking of individual cells may be hard and impractical. In such cases, other methods like optical flow and particle image velocimetry (PIV) can be used to get a velocity field of the cells (124). PIV was originally introduced

in fluid mechanics and required the addition of particles that were statistically traced over time to obtain a velocity field (125), but in biology, points of interest may be identified within the tissue and used to perform PIV (126,127). Optical flow works in a similar way as PIV, but rather than matching discrete locations, the overall grayscale intensity profile is matched over a certain window. Among the applications of PIV and optical flow in biology are the motion of epithelial cells (128,129) and invasion of cancerous tissue (130,131). For a deeper description and discussion about the PIV and optical flow, we would like to point the reader to a recent review on the use of these techniques in the description of cellular systems by Vig et al. (124). The velocity map that is the result of these methods allows studies of certain measures such as speed, direction of the migration, and cell-to-cell correlations, which are quantities of focus in collective cell migration independently of the tracking method (1,126,132). The stochastic component is normally a less interesting feature in collective migration than in single cell migration, partly because the component is smaller and partly because the study of collective migration is focused on the asymptotic behavior of the population of cells. Studies on collective migration investigate the differences in migration under external manipulation and/or the underlying mechanisms for the collective migration (133). We exemplify collective migration by the following three commonly used example systems: wound healing (4,60,134), neural crest cell migration (2,135), and *Drosophila* gastrulation (136).

Wound healing is often considered to be a one-dimensional process with the wound scratch assay being the predominant method (60,137). In wound scratch assays, an epithelial layer is damaged creating a void, and then the speed and manner of cells filling this void are recorded. This one-dimensional description is often a sufficient model to investigate certain aspects of wound healing, such as the effect of different wavelength LED light on the time to wound closure (138). In some studies, the 2D velocity map was considered even if the wound is practically one dimensional (126,127). There are also a few studies that considered the full 3D environment during wound healing to better clarify the proliferation and migration of cells in wound healing (4). Also, in 2D and 3D studies of wound healing, the speed of directed migration and time to wound closing are the main measures that are considered. As wounds are a damage of tissue, it is obvious that mechanistic forces between the cells in the tissue are a strong factor in driving the collective migration (60,62). Besides migration, cell proliferation is an important factor in wound healing and the proliferation has been shown to partly be the driving force behind the observed migration (139).

The migration of neural crest cells is a key event in the development of the cortex in vertebrates, and erroneous migration may result in cortical dysplasia syndromes such as lissencephaly in humans (140,141). While mechanistic forces play a role in this migration, the main factor in this system is the migration along morphogen gradients (142). Morphogen gradients are thought to be pre-existing signals that guide the development of organs or entire organisms (143). The mechanisms underlying the generation and sustainability of such gradients are an ongoing research topic and if a sufficient gradient can be maintained the collective movement observed may simply be chemotaxis (3,143). An alternative hypothesis is that the migrating cells themselves are creating local gradients by binding and internalizing molecules that are not necessarily organized in a graded way (2,144). After internalization of the molecules, the cells change their local environment by breaking down lysophosphatidic acid, thereby creating a gradient in an otherwise homogeneous environment (145). In the zebrafish, this has been modeled to demonstrate that such a dynamic gradient can explain long range collective migration (146). The cells that create the local gradient are examples of leader cells; those are generally speaking cells that are driving the collective migration, thereby dragging along the other cells that are known as followers (123).

In *Drosophila* flies, which is the model system for entire organism morphogenesis, it has been shown that fixed morphogen gradients are present and stable (143,147). The gastrulation of *Drosophila* is a 2 h process where approximately 6,000 cells undergo proliferation, reorganization, differentiation, and migration (1). As discussed earlier, cell-to-cell correlations is an important measure to study the system (148), and also the dynamics of cell area and morphology of the cells have been used to elucidate the forces that act on cells under different conditions (149). In most of the articles on collective movement, the measures are time averaged. However, there are cases where the dynamics of processes has to be considered. An example of dynamic analysis in the case of *Drosophila* is the study by Martin et al. who showed that the gastrulation is an oscillatory process where the contraction of cells is driven by a dynamic actin-myosin network (150). In this study, it was shown that the constriction of epithelial cells is asynchronous between neighboring cells and the actin–myosin network is stabilizing the system providing a net constriction. Also, in wound healing and collective migration of epithelial cells, time resolved analysis has uncovered that the collective migration is happening in bursts rather than with a constant speed (151,152). Such details are lost when considering the time average of the system.

Role of the ECM

In 2D migration experiments, whether it is a scratch assay (137) or phagocyte-pathogen assays (7), the environment in which the cells can move is usually homogeneous. An in vivo environment is normally not so homogeneous, the largest single affecting factor seems to be the ECM (119,123,153,154). As we discussed earlier, Wu et al. (93) demonstrated that heterogeneity of cell motility explained the departure from a PRW model in 2D, but in 3D, this is not sufficient. In a subsequent article from the group, the role of the ECM was further investigated and an anisotropic analysis framework was presented (119). The group also demonstrated that fiber alignments and pore sizes in the ECM strongly correlate with cell motility (154). It is also the case that the placement of cells on a flat surface changes cell geometry and

migration mode (155). In a 2D environment cells are flat and move with the help of lamellipodia, while in 3D, the cells are more spherical and migrate using blebs giving rise to different migration modes (156).

The structure in vivo is naturally hard to control, and therefore, attempts to investigate the effects of different geometries in vitro have been made both in 2D (59) and in 3D (154). The latter is naturally more relevant when comparing with the in vivo situation, but the experimental reality in 3D is that structural properties are entangled. A manipulation of the ECM stiffness, the most studied structural quality, also changes the ligand density (17). In the dissemination of cancer, it is known that leader cells degrade the ECM and create tunnels which follower cells can migrate through and create metastases (157,158). In tumor dissemination, it is naturally desirable to slow down the migration process to contain tumors, but as discussed, the cell migration may involve different mechanisms and pathways in 2D and 3D (159). It is therefore not certain that pathways that were described as fundamental for cancer cell migration in vitro are equally important in vivo (160). To have any possibility of comparing migration from different in vivo experiments, it is absolutely necessary that full information of the environment in which the cell is migrating is provided (14).

Discussion and Future Challenges

This review has given an overview of methods and systems that are used to investigate and quantify cell migration both at the level of individual tracks and at the level of populations. Measures, models, and visualizations are routinely used to distinguish between conditions (13,27,92,138) and to unravel mechanisms driving migration (17,150,151,161). Models have also been used to describe the migration patterns of cells, for example, if cells can be described by a PRW (67,90,162), a Lévy walk (9,104,107), or more exotic stochastic models (39,118,119). Also, measures and combinations of measures have been used to generally quantify the migration type, for example, to distinguish between straight walkers and spatially confined cells (76,83). Just as for general image analysis and tracking, track analysis pipelines are highly specialized for each specific task. The most "standard" approaches in track analysis are probably meandering index, mean squared displacement (MSD), and PRW models.

One hurdle for scientists that are not experts at programming and data analysis is that there is no standard software built with flexibility and user friendliness as the major focus. A challenge for researchers is therefore to develop software and modules for track analysis that are both flexible and user-friendly. A number of commercial and open-source software tools are available. In their review from 2012, Meijering et al. list over 30 software tools and the numbers are growing (65). Some of the major commercial programs for tracking, such as Volocity (PerkinElmer Inc., Waltham, MA) and Imaris (Bitplane AG, Zurich, Switzerland), as well as open-source alternatives, for example, ImageJ (18,161,163,164) and Icy (165), have some ability to perform track analysis. An interesting end-to-end platform for both tracking and analysis is CellMissy (68,166) that allows calculations of many of the measures that are listed in Table 1. Currently, CellMissy is restricted to 2D, although the program has a modular structure which may allow for future developments. An extremely interesting tool is the recently launched MotilityLab (http://www.motilitylab.net/), which allows researchers to plot and analyze track data directly in the browser. MotilityLab is also available for the statistically oriented programming language R (167).

When trying to find information on measures, their definitions, and what information they provide the lack of a common vocabulary is a real issue. We have already mentioned this at the beginning of this review, and we have pointed out cases of naming ambiguities throughout the review. An even more important issue than a common vocabulary is the availability of data and code. To openly share your data, either as tracks or as raw videos, allows other researchers to check their methods and possibly investigate if other measures or models can reveal additional information. A concrete example would be the opportunity for researchers developing methods that can describe a BPRW (114–116). With access to large amount of data, the researchers can check that the asymptotic solutions are valid for a range of biologically relevant cases. Besides biological data, such repositories could also include synthetic tracks or code that produces them. This gives researchers a possibility to test their methods on data where ground truth is known and biological as well as experimental parameters can be easily varied. Such a parameter can, for example, refer to how frame rate affects a given measure and how to compensate for different frame rates. There are currently a few projects aimed at providing dictionaries for tracks and track analysis as well as repositories for tracking data (32). Among the most proficient are the Cell Migration Gateway (http://www.cellmigration.org/) and the Cell Migration Standardisation Organisation (https://cmso.science/). The establishment of a common vocabulary for tracks simplifies comparisons between studies, and openly available data make it possible to test how well a newly developed analysis method generalizes.

As intravital microscopy becomes more and more common (168), the demand for 3D in vivo track analysis will also increase. Many studies suggest that the migration mechanisms and patterns are completely different between 2D in vitro experiments and 3D in vivo assays (93,159,160). The most important factor for in vivo migration seems to be the ECM (17,153,154). This will surely require that at least the environment in which the tracks are recorded is well described geometrically and biophysically. With that information, there is a chance to decouple the movement of cells based on signaling and the motion that is affected by the environment. Without this information it is not possible to decouple the observed migration from, for example, ECM fiber orientation, and evaluate the effect of antimigratory drugs (14). It is therefore quite possible that the analysis of cell tracks may divide into approaches that are proven to work well in vitro, such as PRW

models, and novel approaches that work well for intravital microscopy.

For collective movement, whether it is the spread of cancerous tissue (131), the gastrulation of *Drosophila* (136), or wound healing (4), we think that future studies will have to take into account both the dynamics of the system's constituents and the three-dimensional nature of tissue. An excellent example of the importance of dynamic properties is the study by Martin et al. who showed that the gastrulation is an oscillatory process (150). Also, in collective motion, the stark differences between in vivo and in vitro systems have to be addressed. An excellent discussion piece in this area is the review by Decaestecker et al. (14) that discusses those challenges with specific focus on antimigratory drugs in cancer research.

Literature Cited

1. Supatto W, Mcmahon A, Fraser SE, Stathopoulos A. Quantitative imaging of collective cell migration during *Drosophila* gastrulation: Multiphoton microscopy and computational analysis. Nat Protoc 2009;4:1397–1412. doi:10.1038/nprot.2009.130.
2. Schumacher LJ, Kulesa PM, McLennan R, Baker RE, Maini PK. Multidisciplinary approaches to understanding collective cell migration in developmental biology. Open Biol 2016;6:160056. doi:10.1098/rsob.160056.
3. Muller P, Rogers KW, Yu SR, Brand M, Schier AF. Morphogen transport. Development 2013;140:1621–1638. doi:10.1242/dev.083519.
4. Safferling K, Sütterlin T, Westphal K, Ernst C, Breuhahn K, James M, Jäger D, Halama N, Grabe N. Wound healing revised: A novel reepithelialization mechanism revealed by in vitro and in silico models. J Cell Biol 2013;203:691–709. doi:10.1083/jcb.201212020.
5. Beltman JB, Maree AF, de Boer RJ. Analysing immune cell migration. Nat Rev Immunol 2009;9:789–798. doi:10.1038/nri2638.
6. Textor J, Henrickson SE, Mandl JN, Von Andrian UH, Rgen Westermann J, De Boer RJ, Beltman JB. Random migration and signal integration promote rapid and robust T cell recruitment. PLoS Comput Biol 2014;10:e1003752. doi:10.1371/journal.pcbi.1003752.
7. Brandes S, Dietrich S, Hünniger K, Kurzai O, Figge MT. Migration and interaction tracking for quantitative analysis of phagocyte–pathogen confrontation assays. Med Image Anal 2017;36:172–183. doi:10.1016/j.media.2016.11.007.
8. Berg HC, Brown DA. Chemotaxis in *Escherichia coli* analyzed by three-dimensional tracking. Nature 1972;239:500–504. doi:10.1159/000395424.
9. Matthäus F, Jagodic M, Dobnikar J. *E. coli* superdiffusion and chemotaxis-search strategy, precision, and motility. Biophys J 2009;97:946–957. doi:10.1016/j.bpj.2009.04.065.
10. Daniels R, Vanderleyden J, Michiels J. Quorum sensing and swarming migration in bacteria. FEMS Microbiol Rev 2004;28:261–289. doi:10.1016/j.femsre.2003.09.004.
11. Sadanandan SK, Baltekin Ö, Magnusson KEG, Boucharin A, Ranefall P, Jaldén J, Elf J, Wählby C. Segmentation and track-analysis in time-lapse imaging of bacteria. IEEE J Sel Top Signal Process 2016;10:174–184. doi:10.1109/JSTSP.2015.2491304.
12. Van Haastert PJM, Bosgraaf L. Food searching strategy of amoeboid cells by starvation induced run length extension. PLoS One 2009;4:e6814. doi:10.1371/journal.pone.0006814.
13. Huang YL, Tung C-K, Zheng A, Kim BJ, Wu M. Interstitial flows promote an amoeboid over mesenchymal motility of breast cancer cells revealed by a three dimensional microfluidic model. Integr Biol 2015;7:1402–1411. doi:10.1039/c5ib00115c.
14. Decaestecker C, Debeir O, Van Ham P, Kiss R. Can anti-migratory drugs be screened in vitro? A review of 2D and 3D assays for the quantitative analysis of cell migration. Med Res Rev 2007;27:149–176. doi:10.1002/med.20078.
15. Wright A, Li Y-H, Zhu C, Woodruff W, Coulter H. The differential effect of endothelial cell factors on in vitro motility of malignant and non-malignant cells. Ann Biomed Eng 2008;36:958–969.
16. Linke F, Harenberg M, Nietert MM, Zaunig S, von Bonin F, Arlt A, Szczepanowski M, Weich HA, Lutz S, Dullin C, et al. Microenvironmental interactions between endothelial and lymphoma cells: A role for the canonical WNT pathway in Hodgkin lymphoma. Leukemia 2016;1–12. doi:10.1038/leu.2016.232.
17. Pathak A, Kumar S. Biophysical regulation of tumor cell invasion: Moving beyond matrix stiffness. Integr Biol 2011;3:267–278. doi:10.1039/c0ib00095g.
18. Linke F, Zaunig S, Nietert MM, von Bonin F, Lutz S, Dullin C, Janovská P, Beissbarth T, Alves F, Klapper W, et al. WNT5A: A motility-promoting factor in Hodgkin lymphoma. Oncogene 2016;36:13–23. doi:10.1038/onc.2016.183.
19. Friedl P, Sahai E, Weiss S, Yamada KM. New dimensions in cell migration. Nat Rev Mol Cell Biol 2012;13:743–747. doi:10.1038/nrm3459.
20. Masuzzo P, Troys M, Van Ampe C, Martens L. Taking aim at moving targets in computational cell migration. Trends Cell Biol 2016;26:88–110. doi:10.1016/j.tcb.2015.09.003.
21. Munoz MA, Biro M, Weninger W. T cell migration in intact lymph nodes in vivo. Curr Opin Cell Biol 2014;30:17–24. doi:10.1016/j.ceb.2014.05.002.
22. Liew PX, Kubes P. Intravital imaging—Dynamic insights into natural killer T cell biology. Front Immunol 2015;6:240. doi:10.3389/fimmu.2015.00240.
23. Schmid B, Shah G, Scherf N, Weber M, Thierbach K, Campos CP, Roeder I, Aanstad P, Huisken J. High-speed panoramic light-sheet microscopy reveals global endodermal cell dynamics. Nat Commun 2013;4:274. doi:10.1038/ncomms3207.
24. Zimmer C. From microbes to numbers: Extracting meaningful quantities from images. Cell Microbiol 2012;14:1828–1835. doi:10.1111/cmi.12032.
25. Rittscher J. Characterization of Biological Processes through Automated Image Analysis. Annu Rev Biomed Eng 2010;12:315–344. doi:10.1146/annurev-bioeng-070909-105235.
26. Medyukhina A, Timme S, Mokhtari Z, Figge MT. Image-based systems biology of infection. Cytometry Part A 2015;87A:462–470. doi:10.1002/cyto.a.22638.
27. Harder N, Batra R, Diessl N, Gogolin S, Eils R, Westermann F, König R, Rohr K. Large-scale tracking and classification for automatic analysis of cell migration and proliferation, and experimental optimization of high-throughput screens of neuroblastoma cells. Cytometry Part A 2015;87A:524–540. doi:10.1002/cyto.a.22632.
28. Nketia TA, Sailema H, Rohde G, Machiraju R, Rittscher J. Analysis of live cell images: Methods, tools and opportunities. Methods 2017;115:65–79.
29. Blanchoin L, Boujemaa-Paterski R, Sykes C, Plastino J. Actin dynamics, architecture, and mechanics in cell motility. Physiol Rev 2014;94:235–263. doi:10.1152/physrev.00018.2013.
30. Danuser G, Allard J, Mogilner A. Mathematical modeling of eukaryotic cell migration: Insights beyond experiments. Annu Rev Cell Dev Biol 2013;29:501–528. doi:10.1146/annurev-cellbio-101512-122308.
31. Mackenzie JA, Nolan M, Insall RH. Local modulation of chemoattractant concentrations by single cells: Dissection using a bulk-surface computational model. Interface Focus 2016;6.
32. Masuzzo P, Martens L, 2014 Cell Migration Workshop Participants. An open data ecosystem for cell migration research. Trends Cell Biol 2015;25:55–58. doi:10.1016/j.tcb.2014.11.005.
33. Zhou H, Yuan Y, Shi C. Object tracking using SIFT features and mean shift. Comput Vis Image Underst 2009;113:345–352. doi:10.1016/j.cviu.2008.08.006.
34. Zhang S, Yao H, Sun X, Lu X. Sparse coding based visual tracking: Review and experimental comparison. Pattern Recogn 2013;46:1772–1788. doi:10.1016/j.patcog.2012.10.006.
35. Tekalp AM. Digital video processing. Second. Pearson Education Inc.; 2015.
36. Meijering E, Dzyubachyk O, Smal I, van Cappellen WA. Tracking in cell and developmental biology. Semin Cell Dev Biol 2009;20:894–902. doi:10.1016/j.semcdb.2009.07.004.
37. Ewers H, Smith AE, Sbalzarini IF, Lilie H, Koumoutsakos P, Helenius A. Single-particle tracking of murine polyoma virus-like particles on live cells and artificial membranes. Proc Natl Acad Sci USA 2005;102:15110–15115. doi:10.1073/PNAS.0504407102.
38. Godinez WJ, Lampe M, Wörz S, Müller B, Eils R, Rohr K. Deterministic and probabilistic approaches for tracking virus particles in time-lapse fluorescence microscopy image sequences. Med Image Anal 2009;13:325–342. doi:10.1016/j.media.2008.12.004.
39. Tejedor V, Benichou O, Voituriez R, Jungmann R, Simmel F, Selhuber-Unkel C, Oddershede LB, Metzler R. Quantitative analysis of single particle trajectories: Mean maximal excursion method. BPJ 2010;98:1364–1372. doi:10.1016/j.bpj.2009.12.4282.
40. Chenouard N, Smal I, de Chaumont F, Maška M, Sbalzarini IF, Gong Y, Cardinale J, Carthel C, Coraluppi S, Winter M, et al. Objective comparison of particle tracking methods. Nat Methods 2014;11:281–289. doi:10.1038/nmeth.2808.
41. Jaiswal A, Godinez WJ, Eils R, Lehmann MJ, Rohr K. Tracking virus particles in fluorescence microscopy images using multi-scale detection and multi-frame association. IEEE Trans Image Process 2015;24:4122–4136. doi:10.1109/TIP.2015.2458174.
42. Brandes S, Mokhtari Z, Essig F, Hünniger K, Kurzai O, Figge MT. Automated segmentation and tracking of non-rigid objects in time-lapse microscopy videos of polymorphonuclear neutrophils. Med Image Anal 2015;20:34–51. doi:10.1016/j.media.2014.10.002.
43. Yang F, Mackey MA, Ianzini F, Gallardo G, Sonka M. Cell segmentation, tracking, and mitosis detection using temporal context. Med Image Comput Comput Assist Interv 2005;8:302–309.
44. Li F, Zhou X, Ma J, Wong STC. Multiple nuclei tracking using integer programming for quantitative cancer cell cycle analysis. IEEE Trans Med Imaging 2010;29:96–105. doi:10.1109/TMI.2009.2027813.
45. Maska M, Ulman V, Svoboda D, Matula P, Matula P, Ederra C, Urbiola A, España T, Venkatesan S, Balak DM, et al. A benchmark for comparison of cell tracking algorithms. Bioinformatics 2014;30:1609–1617. doi:10.1093/bioinformatics/btu080.
46. Padfield D, Rittscher J, Roysam B. Coupled minimum-cost flow cell tracking for high-throughput quantitative analysis. Med Image Anal 2011;15:650–668. doi:10.1016/j.media.2010.07.006.
47. Chenouard N, Bloch I, Olivo-Marin J. Multiple hypothesis tracking for cluttered biological image sequences. IEEE Trans Pattern Anal Mach Intell 2013;35:2736–3750. doi:10.1109/TPAMI.2013.97.
48. Magnusson KEG, Jalden J. A batch algorithm using iterative application of the Viterbi algorithm to track cells and construct cell lineages. In: 2012 9th IEEE International Symposium on Biomedical Imaging. IEEE; 2012. pp 382–385. doi:10.1109/ISBI.2012.6235564.
49. Mukherjee DP, Ray N, Acton ST. Level set analysis for leukocyte detection and tracking. IEEE Trans Image Process 2004;13:562–572. doi:10.1109/TIP.2003.819858.
50. Ray N, Acton ST, Ley K. Tracking leukocytes in vivo with shape and size constrained active contours. IEEE Trans Med Imaging 2002;21. doi:10.1109/TMI.2002.806291.

51. Huth J, Buchholz M, Kraus JM, Schmucker M, Von Wichert G, Krndija D, Seufferlein T, Gress TM, Kestler HA. Significantly improved precision of cell migration analysis in time-lapse video microscopy through use of a fully automated tracking system. BMC Cell Biol 2010;11.
52. Baker RM, Brasch ME, Manning ML, Henderson JH. Automated, contour-based tracking and analysis of cell behaviour over long time scales in environments of varying complexity and cell density. J R Soc Interface 2014;11:20140386. doi:10.1098/rsif.2014.0386.
53. Zimmer C, Labruyère E, Meas-Yedid V, Guillén N, Olivo-Marin J-C. Segmentation and tracking of migrating cells in videomicroscopy with parametric active contours: A tool for cell-based drug testing. IEEE Trans Med Imaging 2002;21. doi:10.1109/TMI.2002.806292.
54. Kass M, Witkin A. Snakes: Active contour models. Int J Comput Vis 1988;321–331.
55. Sliusarenko O, Heinritz J, Emonet T, Jacobs-Wagner C. High-throughput, subpixel precision analysis of bacterial morphogenesis and intracellular spatio-temporal dynamics. Mol Microbiol 2011;80:612–627. doi:10.1111/j.1365-2958.2011.07579.x.
56. Coller KE, Berger KL, Heaton NS, Cooper JD, Yoon R, Randall G. RNA interference and single particle tracking analysis of hepatitis C virus endocytosis. PLoS Pathog 2009;5:e1000702. doi:10.1371/journal.ppat.1000702.
57. Haug AJ. Bayesian Estimation and Tracking: A Practical Guide. Hoboken, New Jersey: Wiley; 2012.
58. Smal I, Draegestein K, Galjart N, Niessen W, Meijering E. Particle filtering for multiple object tracking in dynamic fluorescence microscopy images: Application to microtubule growth analysis. IEEE Trans Med Imaging 2008;27(6):789–804. doi:10.1109/TMI.2008.916964.
59. Vedula SRK, Leong MC, Lai TL, Hersen P, Kabla AJ, Lim CT, Ladoux B. Emerging modes of collective cell migration induced by geometrical constraints. Proc Natl Acad Sci USA 2012;109:12974–12979. doi:10.1073/pnas.1119313109.
60. Vedula SRK, Ravasio A, Lim CT, Ladoux B. Collective cell migration: A mechanistic perspective. Physiology 2013;28:370–379. doi:10.1152/physiol.00033.2013.
61. Foxman EF, Kunkel EJ, Butcher EC. Integrating conflicting chemotactic signals. J Cell Biol 1999;147:577–588.
62. Parent CA, Weiner OD. The symphony of cell movement: How cells orchestrate diverse signals and forces to control migration. Curr Opin Cell Biol 2013;25:523–525. doi:10.1016/j.ceb.2013.07.011.
63. Li L, Nørrelykke SF, Cox EC. Persistent cell motion in the absence of external signals: A search strategy for eukaryotic cells. PLoS One 2008;3:e2093. doi:10.1371/journal.pone.0002093.
64. Dunn GA, Brown AF. A unified approach to analysing cell motility. J Cell Sci Suppl 1987;8:81–102.
65. Meijering E, Dzyubachyk O, Smal I. Methods for cell and particle tracking. Methods Enzymol 2012;504:183–200. doi:10.1016/B978-0-12-391857-4.00009-4.
66. Uhlenbeck GE, Ornstein LS. On the theory of the Brownian motion. Phys Rev 1930;36:823–841. doi:10.1103/PhysRev.36.823.
67. Campos D, Méndez V, Llopis I. Persistent random motion: Uncovering cell migration dynamics. J Theor Biol 2010;267:526–534. doi:10.1016/j.jtbi.2010.09.022.
68. Masuzzo P, Huyck L, Simiczyjew A, Ampe C, Martens L, Van Troys M. An end-to-end software solution for the analysis of high-throughput single-cell migration data. Sci Rep 2017;7:42383. doi:10.1038/srep42383.
69. Qian H, Sheetz MP, Elson EL. Single particle tracking. Analysis of diffusion and flow in two-dimensional systems. Biophys J 1991;60:910–921. doi:10.1016/S0006-3495(91)82125-7.
70. Ferrari R, Manfroi AJ, Young WR. Strongly and weakly self-similar diffusion. Phys D 2001;154:111–137.
71. Sbalzarini IF, Koumoutsakos P. Feature point tracking and trajectory analysis for video imaging in cell biology. J Struct Biol 2005;151:182–195. doi:10.1016/j.jsb.2005.06.002.
72. Codling EA, Plank MJ, Benhamou S. Random walk models in biology. J R Soc Interface 2008;5:813–834. doi:10.1098/rsif.2008.0014.
73. Kime D, Ebrahimi M, Nysten K, Roelants I, Rurangwa E, Moore HD, Ollevier F. Use of computer assisted sperm analysis (CASA) for monitoring the effects of pollution on sperm quality of fish; application to the effects of heavy metals. Aquat Toxicol 1996;36:223–237. doi:10.1016/S0166-445X(96)00806-5.
74. Larsen M, Wei C, Yamada KM. Cell and fibronectin dynamics during branching morphogenesis. J Cell Sci 2006;119:3376–3384. doi:10.1242/jcs.03079.
75. Figge MT, Meyer-Hermann M. Modelling intravital two-photon data of lymphocyte migration and interaction. In: Molina-Paris C, Lythe G, editors. Mathematical Models and Immune Cell Biology. Springer: New York, Dordrecht, Heidelberg, London; 2011. p 12139. doi:10.1007/978-1-4419-7725-0_6.
76. Mokhtari Z, Mech F, Zitzmann C, Hasenberg M, Gunzer M, Figge MT. Automated characterization and parameter-free classification of cell tracks based on local migration behavior. PLoS One 2013;8:e80808. doi:10.1371/journal.pone.0080808.
77. Worbs T, Mempel TR, Bölter J, von Andrian UH, Förster R. CCR7 ligands stimulate the intranodal motility of T lymphocytes in vivo. J Exp Med 2007;204:489–495. doi:10.1084/jem.20061706.
78. Coelho FM, Natale D, Soriano SF, Hons M, Swoger J, Mayer J, Danuser R, Scandella E, Pieczyk M, Zerwes H-G, et al. Naive B-cell trafficking is shaped by local chemokine availability and LFA-1-independent stromal interactions. Blood 2013;121:
79. Figge MT, Garin A, Gunzer M, Kosco-Vilbois M, Toellner K-M, Meyer-Hermann M. Deriving a germinal center lymphocyte migration model from two-photon data. J Exp Med 2008;205:3019–3029. doi:10.1084/jem.20081160.
80. Meyer-Hermann M, Figge MT, Toellner K-M. Germinal centres seen through the mathematical eye: B-cell models on the catwalk. Trends Immunol 2009;30:157–164. doi:10.1016/j.it.2009.01.005.
81. Colvin RA, Means TK, Diefenbach TJ, Moita LF, Friday RP, Sever S, Campanella GS, Abrazinski T, Manice LA, Moita C, et al. Synaptotagmin-mediated vesicle fusion regulates cell migration. Nat Immunol 2010;11:495–502. doi:10.1038/ni.1878.
82. Harley BAC, Kim H-D, Zaman MH, Yannas IV, Lauffenburger DA, Gibson LJ. Microarchitecture of three-dimensional scaffolds influences cell migration behavior via junction interactions. Biophys J 2008;95:4013–4024. doi:10.1529/biophysj.107.122598.
83. Lan T, Cheng K, Ren T, Arce SH, Tseng Y. Displacement correlations between a single mesenchymal-like cell and its nucleus effectively link subcellular activities and motility in cell migration analysis. Sci Rep 2016;6:34047. doi:10.1038/srep34047.
84. Einstein A. Über die von der molekularkinetischen Theorie der Wärme geforderte Bewegung von in ruhenden Flüssigkeiten suspendierten Teilchen. Ann Phys 1905;322:549–560. doi:10.1002/andp.19053220806.
85. Fürth R. Einige Untersuchungen über Brownsche Bewegung an einem Einzelteilchen. Ann Phys 1917;358:177–213. doi:10.1002/andp.19173581102.
86. Selmeczi D, Li L, Pedersen LII, Nrrelykke SF, Hagedorn PH, Mosler S, Larsen NB, Cox EC, Flyvbjerg. Cell motility as random motion: A review. Eur Phys J Spec Top 2008;157:1–15. doi:10.1140/epjst/e2008-00626-x.
87. Stokes CL, Lauffenburger DA, Williams SK. Migration of individual microvessel endothelial cells: Stochastic model and parameter measurement. J Cell Sci 1991;99:419–430.
88. Marathe R, Meel C, Schmidt NC, Dewenter L, Kurre R, Greune L, Schmidt MA, Müller MJI, Lipowsky R, Maier B, Klumpp S. Bacterial twitching motility is coordinated by a two-dimensional tug-of-war with directional memory. Nat Commun 2014;5:doi:10.1038/ncomms4759.
89. Gail MH, Boone CW. The locomotion of mouse fibroblasts in tissue culture. Biophys J 1970;10:980–993. doi:10.1016/S0006-3495(70)86347-0.
90. Selmeczi D, Mosler S, Hagedorn PH, Larsen NB, Flyvbjerg H. Cell motility as persistent random motion: Theories from experiments. Biophys J 2005;89:912–931. doi:10.1529/biophysj.105.061150.
91. Dieterich P, Klages R, Preuss R, Schwab A. Anomalous dynamics of cell migration. Proc Natl Acad Sci USA 2008;105:459–463. doi:10.1073/pnas.0707603105.
92. Takagi H, Sato MJ, Yanagida T, Ueda M, Ben-Jacob E. Functional analysis of spontaneous cell movement under different physiological conditions. PLoS One 2008;3:e2648. doi:10.1371/journal.pone.0002648.
93. Wu P-H, Giri A, Sun SX, Wirtz D. Three-dimensional cell migration does not follow a random walk. Proc Natl Acad Sci USA 2014;111:3949–3954. doi:10.1073/pnas.1318967111.
94. Huang S, Brangwynne CP, Parker KK, Ingber DE. Symmetry-breaking in mammalian cell cohort migration during tissue pattern formation: Role of random-walk persistence. Cell Motil Cytoskeleton 2005;61:201–213. doi:10.1002/cm.20077.
95. Reynolds AM. Adaptive Lévy walks can outperform composite Brownian walks in non-destructive random searching scenarios. Phys A 2009;388:561–564. doi:10.1016/j.physa.2008.11.007.
96. Zaburdaev V, Denisov S, Klafter J. Lévy walks. Rev Mod Phys 2015;87:483–530. doi:10.1103/RevModPhys.87.483.
97. Harris TH, Banigan EJ, Christian DA, Konradt C, Wojno EDT, Norose K, Wilson EH, John B, Weninger W, Luster AD, et al. Generalized Lévy walks and the role of chemokines in migration of effector CD8+ T cells. Nature 2012;486:545–548. doi:10.1038/nature11098.
98. Benhamou S. How many animals really do the Lévy walk? Ecology 2007;88:1962–1969. doi:10.1890/06-1769.1.
99. Plank M, James A. Optimal foraging: Lévy pattern or process? J R Soc Interface 2008;5.
100. Pyke GH. Understanding movements of organisms: It's time to abandon the Lévy foraging hypothesis. Methods Ecol Evol 2015;6:1–16. doi:10.1111/2041-210X.12298.
101. Plank MJ, Auger-Méthé M, Codling EA. Lévy or not? Analysing positional data from animal movement paths. Berlin/Heidelberg: Springer; 2013. pp 33–52. doi:10.1007/978-3-642-35497-7_2.
102. Auger-Méthé M, Derocher AE, Plank MJ, Codling EA, Lewis MA. Differentiating the Lévy walk from a composite correlated random walk. Methods Ecol Evol 2015;6:1179–1189. doi:10.1111/2041-210X.12412.
103. Codling EA, Bearon RN, Thorn GJ. Diffusion about the mean drift location in a biased random walk. Ecology 2010;91:3106–3113.
104. Ariel G, Rabani A, Benisty S, Partridge JD, Harshey RM, Be'er A. Swarming bacteria migrate by Lévy Walk. Nat Commun 2015;6:8396. doi:10.1038/ncomms9396.
105. Reynolds AM, Ouellette NT. Swarm dynamics may give rise to Lévy flights. Sci Rep 2016;6:30515. doi:10.1038/srep30515.
106. Matthäus F, Mommer MS, Curk T, Dobnikar J. On the origin and characteristics of noise-induced Lévy walks of *E. coli*. PLoS One 2011;6:e18623. doi:10.1371/journal.pone.0018623.
107. Reynolds AM. Can spontaneous cell movements be modelled as Lévy walks? Phys A 2010;389:273–277. doi:10.1016/j.physa.2009.09.027.
108. van Haastert PJM, Postma M. Biased random walk by stochastic fluctuations of chemoattractant–receptor interactions at the lower limit of detection. Biophys J 2007;93:1787–1796. doi:10.1529/biophysj.107.104356.
109. Taylor HB, Liepe J, Barthen C, Bugeon L, Huvet M, Kirk PDW, Brown SB, Lamb JR, Stumpf MPH, Dallman MJ, et al. P38 and JNK have opposing effects on persistence of in vivo leukocyte migration in zebrafish. Immunol Cell Biol 2013;91:60–69. doi:10.1038/icb.2012.57.
110. Liepe J, Sim A, Weavers H, Ward L, Martin P, Stumpf MPH. Accurate reconstruction of cell and particle tracks from 3D live imaging data. Cell Syst 2016;3:102–107. doi:10.1016/j.cels.2016.06.002.

111. Alt W. Biased random walk models for chemotaxis and related diffusion approximations. J Math Biol 1980;9:147–177. doi:10.1007/BF00275919.
112. Textor J, Peixoto A, Henrickson SE, Sinn M, von Andrian UH, Westermann J. Defining the quantitative limits of intravital two-photon lymphocyte tracking. Proc Natl Acad Sci USA 2011;108:12401–12406. doi:10.1073/pnas.1102288108.
113. Banigan EJ, Harris TH, Christian DA, Hunter CA, Liu AJ. Heterogeneous CD8+ T cell migration in the lymph node in the absence of inflammation revealed by quantitative migration analysis. PLoS Comput Biol 2015;11:1–20. doi:10.1371/journal.pcbi.1004058.
114. Keller JB. Diffusion at finite speed and random walks. Proc Natl Acad Sci USA 2004;101:1120–1122. doi:10.1073/pnas.0307052101.
115. Belousov R, Cohen EGD, Rondoni L. Langevin equation for systems with a preferred spatial direction. Phys Rev E 2016;94:32127. doi:10.1103/PhysRevE.94.032127.
116. Masoliver J. Fractional telegrapher's equation from fractional persistent random walks. Phys Rev E 2016;93:doi:10.1103/PhysRevE.93.052107.
117. Hill NA, Häder D-P. A biased random walk model for the trajectories of swimming micro-organisms. J Theor Biol 1997;186:503–526. doi:10.1006/jtbi.1997.0421.
118. Metzner C, Mark C, Steinwachs J, Lautscham L, Stadler F, Fabry B. Superstatistical analysis and modelling of heterogeneous random walks. Nat Commun 2015;6:7516. doi:10.1038/ncomms8516.
119. Wu P-H, Giri A, Wirtz D. Statistical analysis of cell migration in 3D using the anisotropic persistent random walk model. Nat Protoc 2015;10:517–527. doi:10.1038/nprot.2015.030.
120. Chauviere A, Preziosi L, Byrne H. A model of cell migration within the extracellular matrix based on a phenotypic switching mechanism. Math Med Biol 2009;27:255–281. doi:10.1093/imammb/dqp021.
121. Jones PJ, Sim A, Taylor HB, Bugeon L, Dallman MJ, Pereira B, Stumpf MP, Liepe J. Inference of random walk models to describe leukocyte migration. Phys Biol 2015;12:66001. doi:10.1088/1478-3975/12/6/066001.
122. Liepe J, Taylor H, Barnes CP, Huvet M, Bugeon L, Thorne T, Lamb JR, Dallman J, Stumpf MPH. Calibrating spatio-temporal models of leukocyte dynamics against in vivo live-imaging data using approximate Bayesian computation. Integr Biol 2012;4:335. doi:10.1039/c2ib00175f.
123. Khalil A, Friedl P. Determinants of leader cells in collective cell migration. Integr Biol (Camb) 2010;2:568–574. doi:10.1039/c0ib00052c.
124. Vig DK, Hamby AE, Wolgemuth CW. On the quantification of cellular velocity fields. Biophys J 2016;110:1469–1475. doi:10.1016/j.bpj.2016.02.032.
125. Melling A. Tracer particles and seeding for particle image velocimetry. Meas Sci Technol 1997;8:1406–1416.
126. Deforet M, Parrini MC, Petitjean L, Biondini M, Buguin A, Camonis J, Silberzan P. Automated velocity mapping of migrating cell populations (AVeMap). Nat Methods 2012;9:1081–1085. doi:10.1038/nmeth.2209.
127. Angelini TE, Hannezo E, Trepat X, Marquez M, Fredberg JJ, Weitz DA. Glass-like dynamics of collective cell migration. Proc Natl Acad Sci USA 2011;108:1714–4719. doi:10.1073/pnas.1010059108/.
128. Zehnder SM, Wiatt MK, Uruena JM, Dunn AC, Sawyer WG, Angelini TE. Multicellular density fluctuations in epithelial monolayers. Phys Rev E 2015;92:32729. doi:10.1103/PhysRevE.92.032729.
129. Ali S, Faraz K, Daul C, Blondel W. Optical flow with structure information for epithelial image mosaicing. In: 2015 37th Annual International Conference of the IEEE Engineering in Medicine and Biology Society. IEEE; 2015. pp 1981–1984. doi:10.1109/EMBC.2015.7318773.
130. Xu Q, Hamilton RJ, Schowengerdt RA, Alexander B, Jiang SB. Lung tumor tracking in fluoroscopic video based on optical flow. Med Phys 2008;35:5351–5359. doi:10.1118/1.3002323.
131. Vransø West A-K, Wullkopf L, Christensen A, Leijnse N, Magelund Tarp J, Mathiesen J, Erler JT, Oddershede LB. Dynamics of cancerous tissue correlates with invasiveness. Sci Rep 2017;7:43800, doi:10.1038/srep43800.
132. Middleton AM, Fleck C, Grima R. A continuum approximation to an off-lattice individual-cell based model of cell migration and adhesion. J Theor Biol 2014;359:220–232. doi:10.1016/j.jtbi.2014.06.011.
133. Mayor R, Etienne-Manneville S. The front and rear of collective cell migration. Nat Rev Mol Cell Biol 2016;17:97–109. doi:10.1038/nrm.2015.14.
134. Poujade M, Grasland-Mongrain E, Hertzog A, Jouanneau J, Chavrier P, Ladoux B, Buguin A, Silberzan P. Collective migration of an epithelial monolayer in response to a model wound. Proc Natl Acad Sci USA 2007;104:15988–15993. doi:10.1073/pnas.0705062104.
135. Szabó A, Mayor R. Modelling collective cell migration of neural crest. Curr Opin Cell Biol 2016;42:22–28. doi:10.1016/j.ceb.2016.03.023.
136. Gorfinkiel N, Schamberg S, Blanchard GB. Integrative approaches to morphogenesis: Lessons from dorsal closure. Genesis 2011;49:522–533. doi:10.1002/dvg.20704.
137. Yarrow JC, Perlman ZE, Westwood NJ, Mitchison TJ. A high-throughput cell migration assay using scratch wound healing, a comparison of image-based readout methods. BMC Biotechnol 2004;4:21. doi:10.1186/1472-6750-4-21.
138. Teuschl A, Balmayor ER, Redl H, van Griensven M, Dungel P. Phototherapy with LED light modulates healing processes in an in vitro scratch-wound model using 3 different cell types. Dermatologic Surg 2015;41:261–268. doi:10.1097/DSS.0000000000000266.
139. Baker RE, Simpson MJ. Models of collective cell motion for cell populations with different aspect ratio: Diffusion, proliferation and travelling waves. Phys A: Stat Mech Its Appl 2012;391:3729–3750. doi:10.1016/j.physa.2012.01.009.
140. Hartmann D, De Strooper B, Saftig P. Presenilin-1 deficiency leads to loss of Cajal–Retzius neurons and cortical dysplasia similar to human type 2 lissencephaly. Curr Biol 1999;9:719–727.
141. Park HT, Wu J, Rao Y. Molecular control of neuronal migration. Bioessays 2002;24:821–827.
142. Woods ML, Carmona-Fontaine C, Barnes CP, Couzin ID, Mayor R, Page KM. Directional collective cell migration emerges as a property of cell interactions. PLoS One 2014;9:e104969. doi:10.1371/journal.pone.0104969.
143. Rogers KW, Schier AF. Morphogen gradients: From generation to interpretation. Annu Rev Cell Dev Biol 2011;27:377–407. doi:10.1146/annurev-cellbio-092910-154148.
144. Tweedy L, Susanto O, Insall RH. Self-generated chemotactic gradients—Cells steering themselves. Curr Opin Cell Biol 2016;42:46–51. doi:10.1016/j.ceb.2016.04.003.
145. Tweedy L, Knecht DA, Mackay GM, Insall RH. Self-generated chemoattractant gradients: Attractant depletion extends the range and robustness of chemotaxis. PLoS Biol 2016;14:e1002404. doi:10.1371/journal.pbio.1002404.
146. Streichan SJ, Valentin G, Gilmour D, Hufnagel L. Collective cell migration guided by dynamically maintained gradients. Phys Biol 2011;8:45004–45008. doi:10.1088/1478-3975/8/4/045004.
147. Eldar A, Dorfman R, Weiss D, Ashe H, Shilo B-Z, Barkai N. Robustness of the BMP morphogen gradient in *Drosophila* embryonic patterning. Nature 2002;419:304–308. doi:10.1038/nature01061.
148. McMahon A, Supatto W, Fraser SE, Stathopoulos A. Dynamic analyses of *Drosophila* gastrulation provide insights into collective cell migration. Science 2008;322:1546–1550.
149. Fischer SC, Blanchard GB, Duque J, Adams RJ, Arias AM, Guest SD, Gorfinkel N. Contractile and mechanical properties of epithelia with perturbed actomyosin dynamics. PLoS One 2014;9:e95695. doi:10.1371/journal.pone.0095695.
150. Martin AC, Kaschube M, Wieschaus EF. Pulsed contractions of an actin–myosin network drive apical constriction. Nature 2009;457:495–499. doi:10.1038/nature07522.
151. Chepizhko O, Giampietro C, Mastrapasqua E, Nourazar M, Ascagni M, Sugni M, Fascio U, Leggio L, Malinverno C, Scita G, et al. Bursts of activity in collective cell migration. Proc Natl Acad Sci USA 2016;113:11408–11413. doi:10.1073/pnas.1600503113.
152. Sharma Y, Vargas DA, Pegoraro AF, Lepzelter D, Weitz DA, Zaman MH. Collective motion of mammalian cell cohorts in 3D. Integr Biol 2015;7:1526–1533. doi:10.1039/C5IB00208G.
153. Nelson CM, Tien J. Microstructured extracellular matrices in tissue engineering and development. Curr Opin Biotechnol 2006;17:518–523. doi:10.1016/j.copbio.2006.08.011.
154. Fraley SI, Wu P-H, He L, Feng Y, Krisnamurthy R, Longmore GD, Wirtz D. Three-dimensional matrix fiber alignment modulates cell migration and MT1-MMP utility by spatially and temporally directing protrusions. Sci Rep 2015;5:14580. doi:10.1038/srep14580.
155. Driscoll MK, Danuser G. Quantifying modes of 3D cell migration. Trends Cell Biol 2015;25:749–759. doi:10.1016/j.tcb.2015.09.010.
156. Paluch EK, Raz E. The role and regulation of blebs in cell migration. Curr Opin Cell Biol 2013;25:582–590. doi:10.1016/j.ceb.2013.05.005.
157. Gaggioli C, Hooper S, Hidalgo-Carcedo C, Grosse R, Marshall JF, Harrington K, Sahai E. Fibroblast-led collective invasion of carcinoma cells with differing roles for RhoGTPases in leading and following cells. Nat Cell Biol 2007;9:1392–1400. doi:10.1038/ncb1658.
158. Patsialou A, Bravo-Cordero JJ, Wang Y, Entenberg D, Liu H, Clarke M, Condeelis JS. Intravital multiphoton imaging reveals multicellular streaming as a crucial component of in vivo cell migration in human breast tumors. Intravital 2013;2:e25294. doi:10.4161/intv.25294.
159. Paul CD, Hung W-C, Wirtz D, Konstantopoulos K. Engineered models of confined cell migration. Annu Rev Biomed Eng 2016;18:159–180. doi:10.1146/annurev-bioeng-071114-040654.
160. Paul CD, Mistriotis P, Konstantopoulos K. Cancer cell motility: Lessons from migration in confined spaces. Nat Rev Cancer 2017;17:131–140.
161. Semmling V, Lukacs-Kornek V, Thaiss CA, Quast T, Hochheiser K, Panzer U, Rossjohn J, Perlmutter P, Cao J, Godfrey DI, et al. Alternative cross-priming through CCL17-CCR4-mediated attraction of CTLs toward NKT cell–licensed DCs. Nat Immunol 2010;11:313–321. doi:10.1038/ni.1848.
162. Sadjadi Z, Shaebani MR, Rieger H, Santen L. Persistent-random-walk approach to anomalous transport of self-propelled particles. Phys Rev E: Stat Nonlin Soft Matter Phys 2015;91:62715. doi:10.1103/PhysRevE.91.062715.
163. Schneider CA, Rasband WS, Eliceiri KW. NIH image to ImageJ: 25 years of image analysis. Nat Methods 2012;9:671–675.
164. Schindelin J, Rueden CT, Hiner MC, Eliceiri KW. The ImageJ ecosystem: An open platform for biomedical image analysis. Mol Reprod Dev 2015;82:518–529. doi:10.1002/mrd.22489.
165. de Chaumont F, Dallongeville S, Chenouard N, Herve N, Pop S, Provoost T, Meas-Yedid V, Pankajakshan P, Lecomte T, Le Montagner Y, et al. Icy: An open bioimage informatics platform for extended reproducible research. Nat Methods 2012;9:690–696. doi:10.1038/nmeth.2075.
166. Masuzzo P, Hulstaert N, Huyck L, Ampe C, Van Troys M, Martens L. CellMissy: A tool for management, storage and analysis of cell migration data produced in wound healing-like assays. Bioinformatics 2013;29:2661–2663. doi:10.1093/bioinformatics/btt437.
167. R Core Team (2014). R: A language and environment for statistical computing. R Foundation for Statistical Computing, Vienna, Austria. http://www.R-project.org/.
168. Masedunskas A, Milberg O, Porat-Shliom N, Sramkova M, Wigand T, Amornphimoltham P, Weigert R. Intravital microscopy: A practical guide on imaging intracellular structures in live animals. Bioarchitecture 2012;2:143–157.